# Rapid speciation in the holopelagic ctenophore *Mnemiopsis* following glacial recession

Authors: Remi N. Ketchum[1,2*], Edward G. Smith[3], Leandra M. Toledo[1], Whitney B. Leach[4], Natalia Padillo-Anthemides[1], Andreas D. Baxevanis[5], Adam M. Reitzel[6], Joseph F. Ryan[1]*

[1] Whitney Laboratory for Marine Bioscience, University of Florida, St. Augustine, Florida, USA
[2] Department of Genetics, University of North Carolina at Chapel Hill, Chapel Hill, North Carolina, USA
[3] School of Life Sciences, The University of Warwick, Coventry, UK
[4] Department of Biological Sciences, Lehigh University, Bethlehem, Pennsylvania, USA
[5] Division of Intramural Research, National Human Genome Research Institute, National Institutes of Health, Bethesda, Maryland, USA
[6] Department of Biological Sciences, University of North Carolina at Charlotte, Charlotte, North Carolina, USA

## Abstract

Understanding how populations diverge is one of the oldest and most compelling questions in evolutionary biology. An in depth understanding of how this process operates in planktonic marine animals, where barriers for gene flow are seemingly absent, is critical to understanding the past, present, and future of ocean life. *Mnemiopsis* plays an important ecological role in its native habitat along the Atlantic coast of the Americas and is highly destructive in its non-native habitats in European waters. Although historical literature described three species of *Mnemiopsis*, the lack of stable morphological characters has led to the collapse of this group into a single species, *Mnemiopsis leidyi*. We generate high-quality reference genomes and use a whole-genome sequencing approach to reveal that there are two species of *Mnemiopsis* along its native range and show that historical divergence between the two species coincides with historical glacial melting. We define a hybridization zone between species and highlight that environmental sensing genes likely contribute to the invasive success of *Mnemiopsis*. Overall, this study provides insights into the fundamental question of how holopelagic species arise without clear barriers to gene flow and sheds light on the genomic mechanisms important for invasion success in a highly invasive species.

## Introduction

Speciation and species delineation is of fundamental importance to evolutionary biology, yet the vast majority of speciation literature is based on terrestrial species with small population sizes, clear physical barriers to gene flow, and external fertilization (1–3). Additionally, what we know about speciation in the ocean is largely dominated by active swimmers with well-developed dispersal abilities (i.e., fish) and coastal epibenthic fauna that are relatively sedentary in their adult stages (4). To better understand mechanisms driving speciation in the oceans, it is critical to expand this set of organisms to include animals that employ a wide range of life history strategies and inhabit other distinct marine ecosystems. Holopelagic invertebrate species spend their entire life in the water column and represent a common suite of life history traits in the ocean with high fecundities (5), large population sizes (6), and high dispersal potential.

*Mnemiopsis* (A. Agassiz, 1865) is a holopelagic genus within the phylum Ctenophora with a native range extending continuously along more than 25,000 kilometers of the Atlantic coast of the Americas from Kittery, Maine to the Valdes Peninsula in Argentina (7–9). These comb jellies are considered one of the 100 most invasive species in the world (10) and their introductions into European waters have triggered community trophic cascades and collapse of fisheries (11). The extensive geographic distribution and invasive abilities of *Mnemiopsis* are driven in part by its broad environmental tolerance (12), flexible planktivorous diet (13), extensive regeneration abilities (14), high fertility levels (15), and a capacity for self-fertilization (16). Risk management for invasive species requires genetic information to establish management units and accurate taxonomic classification is a fundamental component of effective control measures.

Despite its rich 100-year history (17) as an evo devo model and the availability of extensive genomics resources (18–21), our understanding of species boundaries in *Mnemiopsis* is subject to debate (22–26). Within the World Register of Marine Species (WoRMS), *Mnemiopsis* is currently divided into two accepted species, *Mnemiopsis leidyi* (A. Agassiz, 1865; type location Massachusetts) and *Mnemiopsis gardeni* (L. Agassiz, 1860; type location South Carolina). A third species, *Mnemiopsis mccradyi* (Mayer, 1900; type location South Carolina) is recognized as a synonym for *Mnemiopsis leidyi* (27). However, there is much confusion as to the ranges and differences in morphology between these two named species and most modern literature considers all ctenophores along the Atlantic and Gulf coasts of the United States as a single species: *Mnemiopsis leidyi* (28). Although there have been previous studies that suggest the possibility of multiple *Mnemiopsis* species (22–26), the molecular data from these studies are based on a limited set of markers and/or limited population sampling and have been insufficient to resolve this question. However, the rapid expansion of next-generation sequencing (NGS) technologies has revolutionized the study of genomic variation within and between species and presents us with a unique opportunity to test for multiple species, revisit the naming system, and explore the evolutionary changes that contribute to invasion success of holopelagic species.

We conducted whole-genome short-read sequencing of 118 individuals from 13 populations within *Mnemiopsis's* native range along the United States Atlantic coast and generated two near chromosome-level genome assemblies of one individual from Florida and one individual from Massachusetts. We used a suite of genomic approaches to understand holopelagic population dynamics, demographic histories, changes in genomic architecture, and evolutionary adaptations. Taken together, these findings highlight barriers to gene flow in holopelagic species, mechanisms underpinning invasion success, and the importance of high spatial resolution sampling in identifying units for invasive species management.

## Results and Discussion

### Whole-genome sequencing of *Mnemiopsis* populations

We sequenced the genomes of 118 *Mnemiopsis* individuals from 13 populations along the US Atlantic coast (Figure 1A, Supplementary Table 1). We generated a total of 730 Gb of Illumina reads and an average genome depth of 18.89x. From this, we generated three datasets that were appropriate for different types of analyses: the All-Sites dataset with 81,758,954 single nucleotide polymorphisms (SNPs), the Population-specific dataset with 3,856,382 SNPs, and an LD-Filtered dataset with 89,750 SNPs.

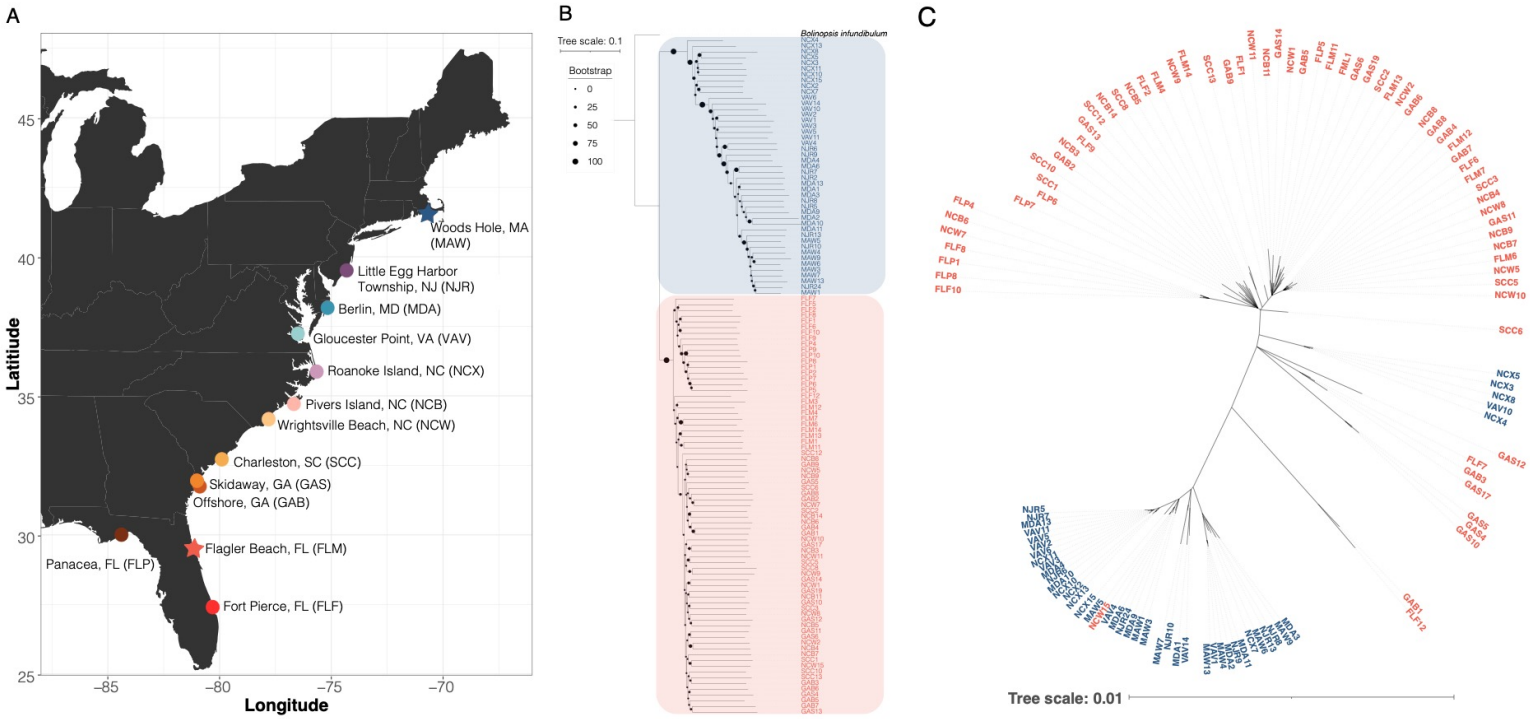


**Figure 1. A)** Sampling map for *Mnemiopsis* collections. Each site is colored according to the MDS plot color scheme with the site abbreviations in parentheses. Stars indicate populations that were sampled for PacBio genome sequencing and assembly. **B)** Phylogenetic tree based on nuclear SNPs, estimated by ngsDist and FastMe using 1,302 SNPs and rooted with *Bolinopsis infundibulum.* The size of the circle on the branch represents the bootstrap support. The northern and southern lineages both receive 100% bootstrap support. The colors of the sample names indicate which lineage the sample belongs to (blue; northern, red; southern). **C)** Mitochondrial genome tree generated using an alignment of the whole mitogenome and IQ-TREE v2.3.2. The colors of the sample names indicate which lineage the sample belongs to.

## Population genomic evidence of two *Mnemiopsis* species

We initially performed phylogenetic analyses using nuclear and mitochondrial markers from our *Mnemiopsis* samples collected along the Atlantic Coast. Our nuclear phylogenetic tree (Figure 1B) revealed the presence of two distinct clades that we will herein refer to as the northern lineage (Roanoke Island, NC to Woods Hole, MA) and the southern lineage (Pivers Island, NC to Panacea, FL). For the most part, these two distinct clades are also observed in our mitochondrial phylogenetic tree (Figure 1C). However, we identified six individuals from populations near the geographic interface of these two clades that exhibit mitonuclear discordance. Specifically, we observed one individual collected at Gloucester Point, Virginia (VAV10) and four individuals

collected in Roanoke Island, North Carolina (NCX3–5,8) with northern nuclear and southern mitochondrial genotypes (Figure 1B–C). Likewise, we observed one individual collected from Wrightsville Beach, North Carolina (NCW15) with southern nuclear and northern mitochondrial genotypes. This level of mitochondrial discordance could be consistent with geographically localized hybridization and adaptive introgression, secondary contact, or demographic disparities such as sex-biased dispersal (29, 30).

To further investigate these patterns, we performed admixture, multidimensional scaling (MDS), and population genetic analyses. We evaluated the presence of 2–7 populations (by adjusting the K parameter) within our dataset using ngsADMIX (31). Setting K=2 separates individuals into northern and southern lineages with the Roanoke Island, NC (NCX) and Gloucester Point, VA (VAV) samples showing signs of admixture (Figure 2A). When K=3, the Roanoke Island samples form their own subpopulation and at higher K values, more substructure within the two lineages becomes evident. MDS plots (Figure 2B) support our ngsADMIX results with the first principal component mirroring the patterns observed in K=2 and accounting for 39.4% of the variance in the data. Our observations of distinct lineages can also be found at the population level, with pairwise $F_{ST}$ comparisons revealing that the average $F_{ST}$ between the northern and southern lineage was 0.278 when the putative hybrid population (Roanoke Island) was included in the northern lineage and 0.315 when it was removed (Table 1). Due to these cumulative results, we also tested for evidence of hybridization in our data using $f_3$ statistics (32). We compared Roanoke Island, NC (NCX) to the northern and southern lineage and notably, this resulted in a negative $f3$ statistic and an absolute Z score >= 3 (threshold used for significance) highlighting that Roanoke Island, NC is a hybrid population (Supplementary Table 2). A recent study (26) detected evidence of hybridization in two populations in Virginia: Gloucester Point and Wachapreague. Because we also sampled from Gloucester Point, we tested for evidence of hybridization in this population by comparing it to the northern and southern lineages (Supplementary Table 3) and did not detect evidence for hybridization. This can likely be explained by the increased statistical power of using 4.8 million SNPs versus the 96 SNPs used for testing in Pujolar et al. 2023 or could be related to temporal shifts in the hybrid zone.

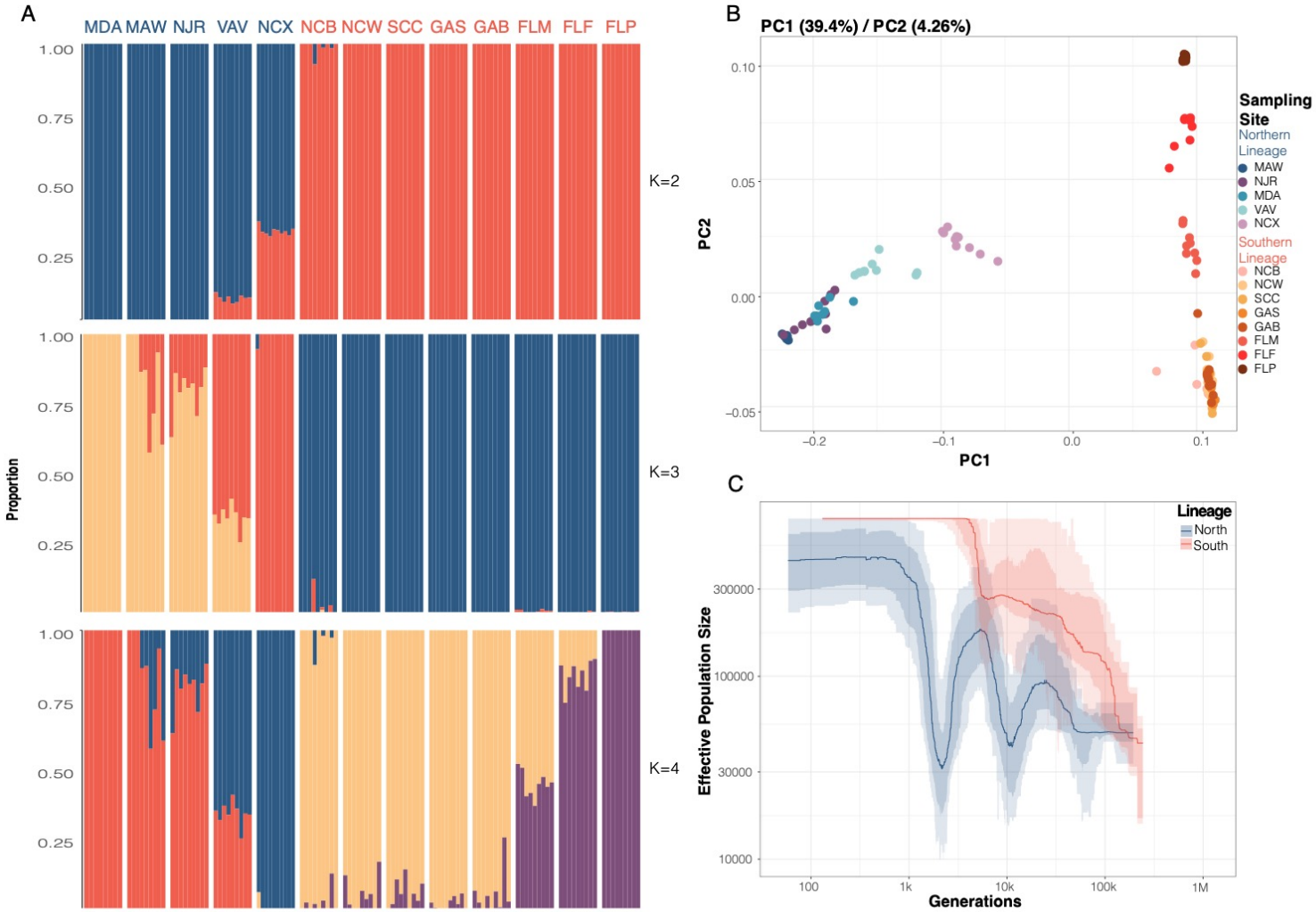


**Figure 2. A)** Admixture plots for the 118 *Mnemiopsis* samples collected for K=2-4 where each bar represents a single individual, and the colors represent each of the K components. **B)** MDS plot for PC1 and PC2 with the percent of total variance explained by each component shown above the plot in parentheses. Samples are colored according to their sampling location with northern lineage samples clustering on the left in blues and purples and southern lineage samples clustering on the right in reds. **C)** Stairway plot results show different demographic histories of the two lineages with generation time of one year and a mutation rate of 6.85 x $10^{-8}$ per base pair per year.

Taken together, our analyses clearly reveal two divergent genetic lineages in US Atlantic *Mnemiopsis*. These results are congruent with evidence of genetic differentiation between Massachusetts and Florida in a previous study (22). However, unlike previous studies, our high-resolution spatial sampling has revealed a clear genetic breakpoint at Roanoke Island, NC. This breakpoint is located where the Gulf Stream leaves the coast and moves offshore into the open Atlantic Ocean. Contrary to expectations for a holopelagic species, we do not find evidence of

gene flow between lineages, except at the hybrid zone. Importantly, this hybrid zone is particularly narrow, with admixture observed at Roanoke Island but absent from Piver's Island, NC located ~200 km away, highlighting that despite their holopelagic nature, clear barriers exist preventing panmixia in *Mnemiopsis*.

**Table 1.** $F_{ST}$ values across all populations of *Mnemiopsis* collected based on the LD-Filtered SNP dataset. These locations included: Woods Hole (MAW), Little Egg Harbor Township (NJR), Berlin (MDA), Gloucester Point (VAV), Roanoke Island (NCX), Pivers Islands (NCB), Wrightsville Beach (NCW), Charleston (SCS), Savannah (GAS), Savannah offshore (GAB), Flagler Beach (FLM), Fort Pierce (FLF), and Panacea (FLP).

| | MAW | NJR | MDA | VAV | NCX | NCB | NCW | SCC | GAS | GAB | FLM | FLF | FLP |
|---|---|---|---|---|---|---|---|---|---|---|---|---|---|
| MAW | X | X | X | X | X | X | X | X | X | X | X | X | X |
| NJR | 0.039 | X | X | X | X | X | X | X | X | X | X | X | X |
| MDA | 0.056 | -0.003 | X | X | X | X | X | X | X | X | X | X | X |
| VAV | 0.215 | 0.097 | 0.075 | X | X | X | X | X | X | X | X | X | X |
| NCX | 0.327 | 0.230 | 0.210 | 0.113 | X | X | X | X | X | X | X | X | X |
| NCB | 0.400 | 0.328 | 0.314 | 0.262 | 0.230 | X | X | X | X | X | X | X | X |
| NCW | 0.402 | 0.330 | 0.317 | 0.266 | 0.235 | 0.001 | X | X | X | X | X | X | X |
| SCC | 0.402 | 0.331 | 0.318 | 0.266 | 0.236 | 0.0003 | 0.0002 | X | X | X | X | X | X |
| GAS | 0.407 | 0.335 | 0.322 | 0.271 | 0.240 | 0.001 | 0.001 | 0.001 | X | X | X | X | X |
| GAB | 0.402 | 0.330 | 0.317 | 0.265 | 0.235 | -0.0003 | 0.001 | 0.00004 | −0.00002 | X | X | X | X |
| FLM | 0.391 | 0.318 | 0.305 | 0.253 | 0.223 | 0.029 | 0.028 | 0.027 | 0.032 | 0.027 | X | X | X |
| FLF | 0.404 | 0.331 | 0.318 | 0.265 | 0.235 | 0.061 | 0.058 | 0.087 | 0.064 | 0.057 | 0.03 | X | X |
| FLP | 0.422 | 0.349 | 0.336 | 0.283 | 0.254 | 0.089 | 0.086 | 0.087 | 0.092 | 0.086 | 0.059 | 0.039 | X |

**Demographic history of *Mnemiopsis***

Stairway plot (33) analysis shows that the demographic histories of *Mnemiopsis* could be traced back from very recent history (<100 generations/years ago) to approximately 100,000 years ago (Figure 2C). The demographic trajectories of the two lineages were remarkably different with the southern lineage experiencing constant population expansion, especially at about 10,000 years ago. The northern lineage has experienced two population bottlenecks, occurring roughly 10,000 years ago and 2,000-3,000 years ago. More recently, the northern lineage is experiencing a population expansion. Interestingly, the split in the effective population size curves between the two lineages occurred ~10,000 years ago which coincides roughly with the retreat of the Laurentide Glacier (by ~8,000 years ago this glacier was confined mostly to Canada) and the flood that was caused when Lake Agassiz burst and flooded several parts of North America, including the northern Atlantic Ocean (34). This influx of cold, freshwater may have reduced the current in the ocean conveyor belt and resulted in less warm seawater traveling poleward and subsequently causing temperatures to drop in the Northern Hemisphere (34, 35). This population size split may have been a result of a reduction in the Gulf Stream current during this time which could have resulted in *Mnemiopsis* to move northward and begin a population expansion as temperatures slowly rose. Finally, the population size decline around 2,000 – 3,000 years ago in the northern lineage may have been caused by the Little Ice Age which occurred ca. 1300-1850 CE (36, 37).

Our results differ from the pairwise sequentially Markovian coalescent (PSMC) results reported in Jaspers et al (22). Although they also reported population expansions about 50,000 generations

ago and a population bottleneck about 1,000-2,000 generations ago, their northern lineage did not show evidence of oscillations in population size. In contrast, ours showed a steady increase in population size beginning at that time. Their southern lineage showed a steady increase in population size from 500,000-50,000 generations ago and then a decrease in population size from then onwards whereas ours has shown a steady increase from 100,000 generations ago to present. The difference in findings can likely be explained by the increased geospatial resolution with our study drawing conclusions from whole-genome level sampling of 5 northern populations and 8 southern populations versus one northern and southern population in the previous study. In addition, while the PSMC method (38) performs well for inferring ancient histories, the Stairway Plot method performs better for inference of more recent population histories and we see the most discordance in our results when looking at more recent population histories (33, 39).

**Structural genomic evidence of speciation**

To investigate genomic differences between the two species, we produced two high-quality, near chromosome-level genome assemblies of one Massachusetts *Mnemiopsis* sample and one Florida sample using PacBio Hifi sequencing technology. When assembled, the Florida genome was 206 Mb and half of the genome was contained in contigs 3.6 Mb or larger (N50). There were 174 contigs total and the 100 largest contigs made up 98% of the assembly. The Massachusetts genome was 215 Mb and half of the genome was contained in contigs 2 Mb or larger. There were 207 contigs total and the 100 largest contigs made up 89% of the assembly. We identified 27,570 and 26,046 protein-coding genes for Florida and Massachusetts, respectively and were able to functionally annotate 27,476 genes for the Florida genome. Benchmarking Universal Single-Copy Orthologs (40) analysis revealed that our assemblies exhibit a similar degree of completeness to other ctenophore genomes (Table 2).

Chromosome-scale linkages of orthologous genes tend to be conserved even over very large time scales (41–45). As such, chromosomal rearrangements are major evolutionary events that can either cause speciation events and/or provide evidence of long periods of isolation between lineages. We conducted macrosynteny analyses to check for evidence of chromosomal rearrangements between the Florida and Massachusetts near-chromosomal genomes. In addition, we compared both genomes to the recently published chromosome-level genome assembly of *Bolinopsis microptera* (44), a lineage that is closely related to *Mnemiopsis* (46). We identified at least one chromosomal rearrangement between the Florida and Massachusetts genomes (Figure 3A-C). The Massachusetts scaffold L006 maps to two Florida scaffolds, G002, which maps completely to Chromosome 1 of *B. microptera*, and G004, which maps completely to chromosome 8 of *B. microptera*. The fact that this linkage group is present in both Florida *Mnemiopsis* and *B. microptera*, suggests that the genomic rearrangement occurred in the Massachusetts lineage. There are potentially other rearrangements involving the Massachusetts scaffolds L012 and L018, but a chromosome-scale assembly would be needed to confirm or refute those possibilities.

223 **Table 2**. Comparison of genome assembly benchmarks between the *Mnemiopsis leidyi* published genome
224 (18) and the two new genome assemblies.

| | *Mnemiopsis leidyi* 2013 | *Mnemiopsis leidyi* 2024 | *Mnemiopsis gardeni* 2024 |
|---|---|---|---|
| Assembly size | 155,865,547 | 215,818,400 | 206,611,897 |
| No. of scaffolds | NA | 5,100 | NA |
| No. of contigs | NA | 207 | 174 |
| Max length (bases) | | 6,852,836 | 9,685,951 |
| N50 | 187,314 (scaff N50) | 2,034,471 (contig N50) | 3,675,794 (contig N50) |
| BUSCO Complete | 204 (80%) | 211 (83%) | 214 (84%) |
| BUSCO Complete + Partial | 233 (91%) | 231 (91 %) | 235 (91 %) |
| BUSCO missing | 22 (8.6%) | 24 (9%) | 20 (8%) |
| BUSCO duplicated | 1.47 | 1.9 | 3.74 |

225

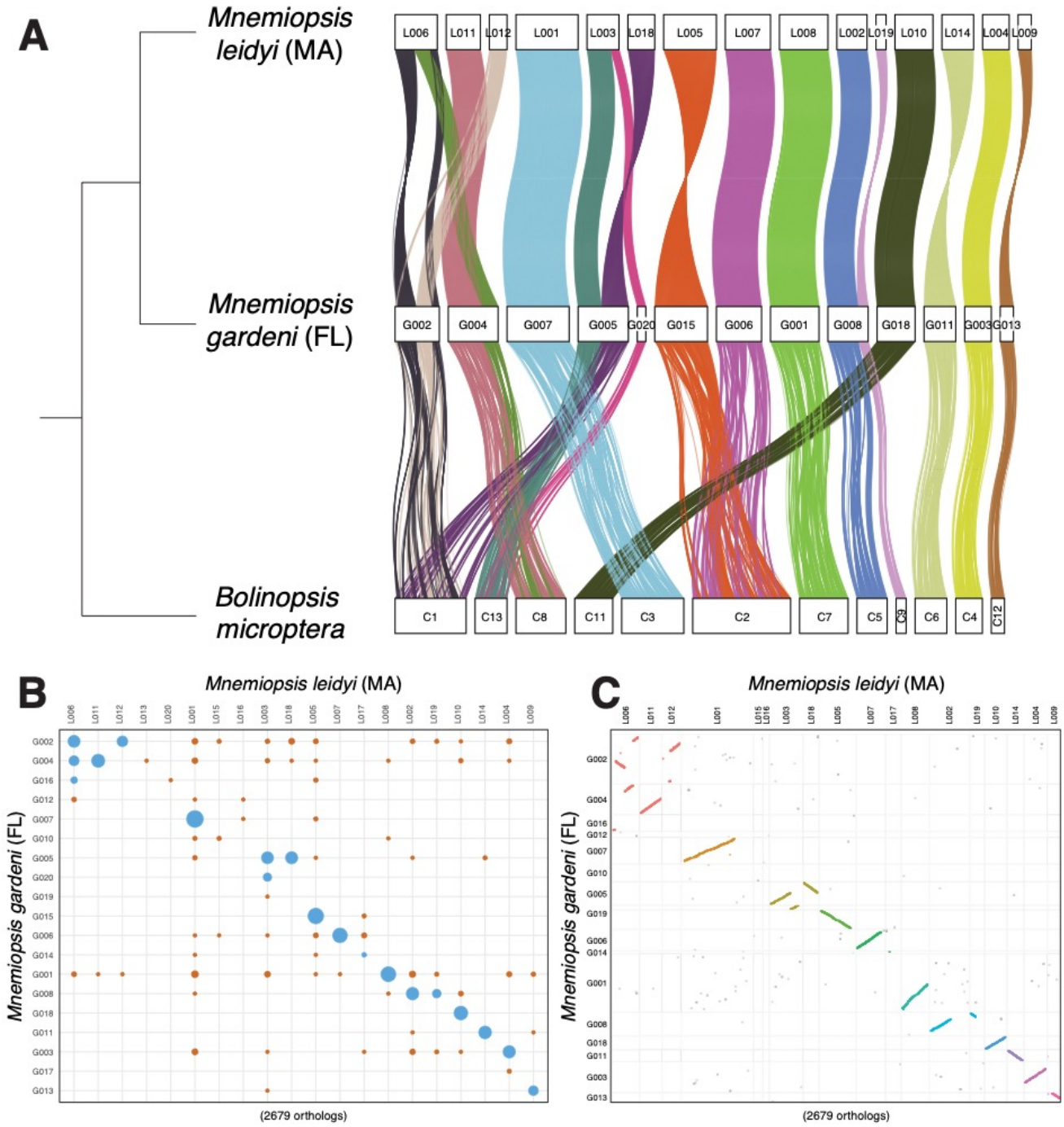


**Figure 3.** Macrosynteny on a near-chromosome scale between *Mnemiopsis leidyi* (top), *M.* gardeni (middle), and *Bolinopsis microptera* (bottom). **(A)** Chord diagram of macrosynteny between *M. leidyi* (MA), *M. gardeni* (FL), and *B. macropteri*. The coordinates of 12,134 orthologs (based on reciprocal best BLAST hits) are plotted. **(B)** Plot of macrosynteny between *M. leidyi* and *M. gardeni*. **(C)** Oxford dot plot between *M. leidyi* (MA) and *M. gardeni* (FL). Each dot represents an ortholog.

232 **The combined evidence supports two species along the US Atlantic coast**
233 Both the population genomic and structural genomic evidence are consistent with there being one
234 species of *Mnemiopsis* (*Mnemiopsis leidyi*) that inhabits the coastal waters stretching from the
235 Outer Banks region of North Carolina to the northern limits of the native range (i.e., at least as
236 north as Woods Hole, MA). Likewise, there is a second species that stretches from at least the Gulf
237 of Mexico to Piver's Island, NC.
238
239 The position of this break corresponds with the location where the swift-flowing Gulf Stream
240 diverges from the North Carolina coast as it collides with the Labrador current (47). This is a
241 known dispersal barrier, and it is thought that these ocean flows are the source of range limits for
242 many species (48). This seems to serve as the likely biogeographic barrier separating *Mnemiopsis*
243 *leidyi* (north) from *Mnemiopsis gardeni* (south). During the last glacial maximum, the Gulf Stream
244 followed its present-day course, but its flow was relaxed by at least 10% (49). As the Laurentide
245 glacier receded and led to a habitat hospitable to *Mnemiopsis*, this reduction of flow may have
246 been sufficient to allow a small founder population to overcome this barrier and these individuals
247 may have initiated the present day *Mnemiopsis leidyi* lineage. A small founding population would
248 be consistent with drastic genomic changes like chromosomal rearrangements being tolerated and
249 spreading to fixation.
250
251 **Genomic signatures of selection in genes mediating environmental sensing**
252 Due to the substantial divergence between these two species, their geographical distribution that
253 spans a significant environmental gradient, and their success as an invasive species, we
254 investigated signatures of selection and local adaptation between the two lineages using the cross-
255 population composite-likelihood ratio (XP-CLR) test (50). To highlight functional categories of
256 these genes, we conducted gene ontology (GO) analysis (51) of the 2,093 genes that overlap with
257 the genomic windows ranked in the top 10% of XP-CLR values. These genes were significantly
258 enriched (P<=0.05) for GO molecular function categories (Table 3). Interestingly, many of these
259 categories include categories associated with sensory processing, neural activity, and/or diet, for
260 example G protein-coupled receptor signaling pathways (P=0.0004), extracellularly glutamate-
261 gated ion channel activity (P=0.012), Golgi vesicle transport (P=0.0078), neurotransmitter
262 transport (P=0.0321), and chitin metabolic processes (P=0.0043).
263
264 The membrane category, which was significantly enriched (P=0.0122), included several key
265 sensory related and neural genes found in regions with high XP-CLR values such as six TRP
266 channels, four glutamate receptors, the single *Mnemiopsis* voltage-gated calcium channel, one of
267 the two *Mnemiopsis* voltage-gated sodium channels, nine voltage-gated potassium channels, two
268 potassium 2-pore domain channels, two calcium channels, a calcium-activated potassium channel,
269 a voltage-gated chloride channel, and two ASIC channels. The chitin metabolic processes category
270 includes two chitinase genes, which are critical for digesting prey. The membrane category also
271 includes syntaxin-6, which is in the genomic region with the highest fixation index of the XP-CLR

272 analysis (Figure 4). Within the XP-CLR outlier regions, we also observe *O*-GLcNAcase (Figure
273 4) which is a post-translational modifier of serine and threonine residues on a wide range of
274 proteins (52). This protein has been associated with stress responses ranging from heat shock to
275 oxidative stress. As both syntaxin-6 and *O*-GLcNAcase have been implicated in modulating
276 autophagic flux in response to nutrient status in *Caenorhabditis elegans* (53, 54), we hypothesize
277 that overwintering in northern populations may be a driver of these selective sweeps as organisms
278 are likely nutrient deficient during this time. In addition, our outlier dataset also contains many
279 other genes that are relevant for nutrient sensing and metabolism such as mechanistic target of
280 rapamycin (mTOR), acetyl coenzyme A synthase, malate dehydrogenase, and cytochrome c
281 oxidase subunit 2. Combined, these results suggest that genes involved in sensing a changing
282 environment and adapting to changes in diet were under high positive selection in the northern
283 lineage as it invaded new environments. This finding provides important candidate genes for future
284 functional verification and sheds light on the importance of nutrient sensing and resilience to
285 nutrient deficiency which may make *Mnemiopsis* such a prolific invader.
286
287 **Table 3.** Gene Ontology (GO) term analysis reveals enrichment in relevant biological processes.

| GO TERM | P-Value | Description |
|---|---|---|
| GO:0005515 | 0 | protein binding |
| GO:0003723 | 0.0002 | RNA binding |
| GO:0004553 | 0.0002 | hydrolase activity |
| GO:0007186 | 0.0004 | G protein-coupled receptor signaling pathway |
| GO:0005215 | 0.001 | transporter activity |
| GO:0005524 | 0.0014 | ATP binding |
| GO:0006468 | 0.0014 | protein phosphorylation |
| GO:0005488 | 0.0014 | binding |
| GO:0004930 | 0.0016 | G protein-coupled receptor activity |
| GO:0004672 | 0.0016 | protein kinase activity |
| GO:0007018 | 0.0039 | microtubule-based movement |
| GO:0006030 | 0.0043 | chitin metabolic process |
| GO:0003755 | 0.0044 | peptidyl-prolyl cis-trans isomerase activity |
| GO:0000413 | 0.0044 | protein peptidyl-prolyl isomerization |
| GO:0007165 | 0.0046 | signal transduction |
| GO:0006366 | 0.0064 | transcription by RNA polymerase II |
| GO:0030117 | 0.0074 | membrane coat |
| GO:0048193 | 0.0078 | Golgi vesicle transport |
| GO:0003676 | 0.0082 | nucleic acid binding |
| GO:0045454 | 0.0083 | cell redox homeostasis |
| GO:0008081 | 0.0098 | phosphoric diester hydrolase activity |

| | | |
|---|---|---|
| GO:0005234 | 0.012 | extracellularly glutamate-gated ion channel activity |
| GO:0016020 | 0.0122 | membrane |
| GO:0055085 | 0.0128 | transmembrane transport |
| GO:0005868 | 0.0143 | cytoplasmic dynein complex |
| GO:0008061 | 0.0147 | chitin binding |
| GO:0009055 | 0.0156 | electron transfer activity |
| GO:0006452 | 0.0157 | translational frameshifting |
| GO:0045905 | 0.0157 | positive regulation of translational termination |
| GO:0045901 | 0.0157 | positive regulation of translational elongation |
| GO:0043022 | 0.0159 | ribosome binding |
| GO:0016462 | 0.0164 | pyrophosphatase activity |
| GO:0016021 | 0.0174 | |
| GO:0005216 | 0.0176 | monoatomic ion channel activity |
| GO:0005096 | 0.019 | GTPase activator activity |
| GO:0010181 | 0.0192 | FMN binding |
| GO:0005978 | 0.0196 | glycogen biosynthetic process |
| GO:0005622 | 0.0198 | intracellular anatomical structure |
| GO:0006811 | 0.0223 | monoatomic ion transport |
| GO:0015035 | 0.0231 | protein-disulfide reductase activity |
| GO:0004970 | 0.0235 | glutamate-gated receptor activity |
| GO:0008017 | 0.0243 | microtubule binding |
| GO:0005576 | 0.0256 | extracellular region |
| GO:0003777 | 0.026 | microtubule motor activity |
| GO:0004252 | 0.0268 | serine-type endopeptidase activity |
| GO:0004177 | 0.0282 | aminopeptidase activity |
| GO:0051056 | 0.0289 | regulation of small GTPase-mediated signal transduction |
| GO:0046933 | 0.0292 | proton-transporting ATP synthase activity |
| GO:0006820 | 0.0311 | monoatomic anion transport |
| GO:0006836 | 0.0321 | neurotransmitter transport |
| GO:0005328 | 0.0326 | neurotransmitter:sodium symporter activity |
| GO:0006810 | 0.033 | transport |
| GO:0016651 | 0.033 | oxidoreductase activity |
| GO:0019001 | 0.0395 | guanyl nucleotide binding |
| GO:0031683 | 0.0395 | G-protein beta/gamma-subunit complex binding |
| GO:0005452 | 0.0398 | solute:inorganic anion antiporter activity |
| GO:0004674 | 0.0412 | protein serine/threonine kinase activity |

| | | |
|---|---|---|
| GO:0006270 | 0.0423 | DNA replication initiation |
| GO:0008603 | 0.0426 | cAMP-dependent protein kinase regulator activity |
| GO:0005952 | 0.0426 | cAMP-dependent protein kinase complex |
| GO:0006383 | 0.0426 | transcription by RNA polymerase III |
| GO:0001932 | 0.0426 | regulation of protein phosphorylation |
| GO:0051287 | 0.0429 | NAD binding |
| GO:0005815 | 0.0442 | microtubule organizing center |
| GO:0046872 | 0.0444 | metal ion binding |
| GO:0005975 | 0.0449 | carbohydrate metabolic process |
| GO:0043130 | 0.0452 | ubiquitin binding |
| GO:0046856 | 0.0455 | phosphatidylinositol dephosphorylation |
| GO:0051920 | 0.0461 | peroxiredoxin activity |

288

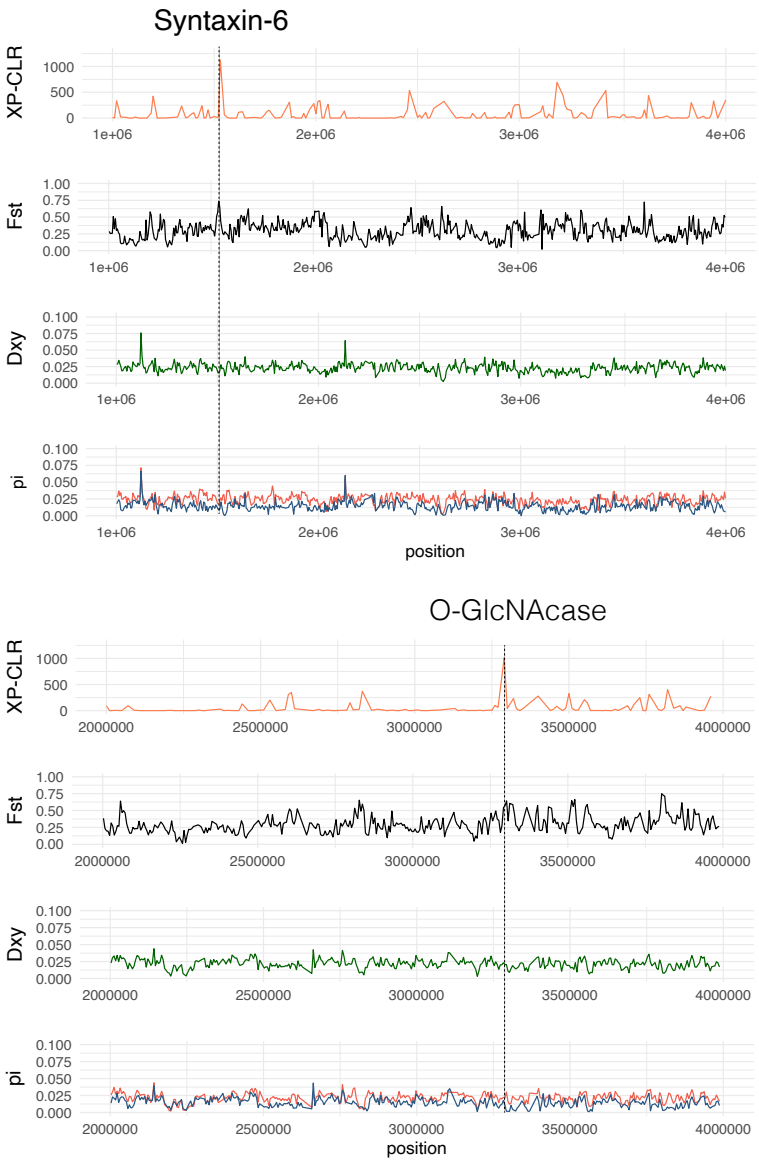


**Figure 4**. The two genes: syntaxin-6 (top) and O-GlcNAcase (bottom) are under selection. The XP-CLR, $F_{ST}$, $D_{XY}$, and nucleotide diversity values were calculated with nonoverlapping 10kb windows and step sizes. The location of the two genes is shown with a dotted gray line.

## Conclusion

Our knowledge of evolution is heavily biased across the tree of life and expansions in taxon sampling often leads to a much richer understanding of how evolutionary forces shape the genomic variation between populations and species. Our findings in the holopelagic ctenophore, *Mnemiopsis* show that despite having life history traits that should promote panmixia (i.e., high fecundity, large population sizes, and high dispersal potential), we instead find evidence of a strong genetic breakpoint that is likely due to barriers created by strong currents off the North Carolina

330 coast. We provide evidence that implicates the retreat of the Laurentide glacier and the subsequent
331 flood of Lake Agassiz in the lineage splitting of the northern and southern species. Finally, we
332 show evidence for selection on environmental sensing genes and genes implicated in surviving
333 stressful conditions, all of which likely contribute to the invasive success of *Mnemiopsis*.
334
335 **Materials and Methods**
336 **Sampling**
337 *Populations*. A total of 118 *Mnemiopsis* samples were collected from thirteen locations along the
338 Atlantic and Gulf coast of the United States. These locations included: Woods Hole (MA), Little
339 Egg Harbor Township (NJ), Berlin (MD), Gloucester Point (VA), Roanoke Island (NC), Pivers
340 Islands (NC), Wrightsville Beach (NC), Charleston (SC), Savannah (GA), Savannah offshore
341 (GA), Flagler Beach (FL), Fort Pierce (FL), and Panacea (FL). Samples were collected between
342 August 2021 and November 2022 from surface waters (<10m) using either a cteno-dipper or a tow
343 net. Samples immediately preserved in ethanol and placed in a -20°C freezer until further
344 processing.
345
346 *Genome*. One *Mnemiopsis* individual was collected from two locations for genome assembly:
347 Woods Hole (MA) and Flagler Beach (FL). These samples were collected in August 2023 from
348 surface waters (<2m) using a cteno-dipper. Samples were preserved in ethanol and placed in a -
349 20°C freezer until further processing.
350
351 **DNA Extraction and Sequencing**
352 *Populations*. High molecular weight DNA was extracted according to the CTAB/Chloroform
353 protocol detailed in Ehrlich et al. 2017 (55). All DNA extractions were visualized on a 1% agarose
354 gel for quality control. One hundred and nineteen individually indexed, paired-end libraries with
355 an approximate insert size of 550 bp were constructed using the NEBNext Ultra II FS DNA Library
356 Preparation kit. Whole-genome sequencing was performed at the University of Florida's ICBR
357 Bioinformatics Core Facility on a NovaSeq6000.
358
359 *Genome*. High molecular weight DNA was extracted using a modified SDS-based lysis described
360 in Moritz et al (55). DNA extractions were visualized on a 1% agarose gel for quality control and
361 quantified using a Qubit dsDNA High Sensitivity Assay Kit on a Qubit 2.0 Fluorometer. Genome
362 sequencing was performed on a Pacific Biosciences Sequel IIe platform, in the Circular Consensus
363 sequencing (CCS) mode. A total of 17.7 - 20.2 Gb of Hifi reads were generated using CCS for the
364 two individuals. PacBio library preparation and sequencing were performed at NIH Intramural
365 Sequence Center (NISC) in Rockville, MD.
366
367 **De novo Genome Assembly**
368 Hifiasm v0.19.8 (56) was used to assemble the two genomes. For the Flagler Beach, FL individual,
369 the `--hom-cov` flag was set to 90. To reduce the amount of duplication, PurgeHaplotigs v1.1.2

370 (57) was run with the 'contigcov' option for low coverage, low point between the peaks, and high
371 coverage cutoffs set to 10, 70, and 175 respectively. The percent cutoff for identifying a contig as
372 a haplotig was set to 50% and this assembly was subsequently run through PurgeHaplotigs 'clip'
373 option that identifies and trims overlapping contig ends. For the Woods Hole, MA individual, the
374 `--hom-cov` flag was set to 101, the 'contigcov' options were set to 25, 70, and 155, and the `-j`
375 and `-s` flags were both set to 55. The percent cutoff `-a` flag was set to 60% and the final assembly
376 was also clipped to remove overlapping contig ends.
377
378 **Gene Prediction and Annotation**
379 Genomic repetitive elements were identified with RepeatModeler v1.0.11 (58) to generate a
380 *Mnemiopsis*-specific repeat element library. Repetitive regions were soft masked prior to gene
381 prediction and annotation using RepeatMasker v4.0.8. We aligned previously published bulk
382 RNA-Seq reads from tissues (PRJEB28334) to the above genome assembly using Bowtie2 (59).
383 Aligned RNA-seq data and gene models for *M. leidyi* (ML2.2.aa) were input into Braker v2.1.5
384 (60). Assembled gene/protein models were functionally annotated using BLASTP v2.9.0+ with
385 three protein databases: UniProt Knowledgebase Swiss-Prot protein models v2021-03, RefSeq
386 invertebrate protein models, and the *M. leidyi* protein models (18). Finally, BUSCO v5 (40) was
387 used to measure the completeness of the genome assembly and protein using the something
388 database.
389
390 **MacrosyntR**
391 We analyzed conserved chromosome-scale synteny (macrosynteny) between these new Florida
392 and Massachusetts *Mnemiopsis* assemblies as well as the published *Bolinopsis microptera* genome
393 assembly. To identify conserved genes, we performed diamond BLAST (61) to compute the
394 reciprocal best BLAST hits between the 2013 ML2.2 *Mnemiopsis* gene models and the gene
395 models of each of the new *Mnemiopsis* assemblies and the published *B. microptera* gene models.
396 These reciprocal best BLAST hits were used to identify significantly conserved macrosyntenic
397 blocks in MacrosyntR (version 0.3.3; (62)).
398
399 **Data processing and filtering of 118 short-read genomes**
400 Raw sequence data was trimmed using Trimmomatic v0.39 (63) with a minimum phred score of
401 33. Once the data was filtered and adaptors were removed, the paired sequences were aligned to
402 the Flagler Beach, FL genome using BWA-mem v0.7.12 (38). Sequence alignments were filtered
403 using Samtools v1.9 (64) for a minimum quality score of 30, Sambamba v0.6.6 (65) was used to
404 filter duplicate reads with default parameters, and bamutil v1.0.15 (66) was used to clip
405 overlapping read pairs.
406
407 We generated three datasets for our different analyses. For each dataset, we used the Flagler Beach,
408 FL genome as our reference and ancestral genome. *LD-Filtered Dataset.* The first was a highly
409 filtered dataset that was produced by using ANGSD v0.921 (67) to call SNPs and estimate

genotype likelihoods using the samtools model (`-GL 1`). We filtered the SNP data for 1) positions that were present in at least 94 out of 118 samples, 2) a maximum coverage of 2360x per site across all individuals to avoid calling sites in highly repetitive regions, 3) a minimum of 354x coverage per site across all individuals, 4) a minimum base quality score <20, 5) a p-value cut off of 10-6 for calling polymorphic loci and 5) retained only SNPs with a minor global allele frequency >5%. The ANGSD output was then subsampled for one SNP out of every 50 and pairwise linkage disequilibrium (LD) was estimated with ngsLD v1.1.1 (68) on this subsampled dataset assuming a maximum distance of 10Kb between SNPs. Linked sites were pruned with the script 'prune_graph.pl' with a maximum distance of 10 Kb between SNPs and a minimum weight of 0.5 (69). The final LD-filtered dataset was used to generate phylogenetic trees, ngsadmix and MDS plots, and calculate $F_{ST}$ measures. *Population-Specific Filtered Dataset.* The second dataset was filtered using the same ANGSD commands as the first dataset (excluding the LD filtering steps) but then underwent a second round of population- specific filtering. Specifically, sampling locations from Woods Hole, MA to Roanoke Island, NC were included in the 'Northern lineage' group and sampling locations from Piver's, NC to Panacea, FL were included in the 'Southern lineage' group. These two groups were filtered separately and for the northern lineage, we filtered the dataset for 1) positions that were present in at least 36 out of 45 individuals, 2) a maximum coverage of 900x coverage per site across all individuals, 3) a minimum of 36x coverage per site across all individuals. For the southern lineage we filtered the dataset for 1) positions that were present in at least 58 out of 73 individuals, 2) a maximum coverage of 1,460x coverage per site across all individuals, 3) a minimum of 175x coverage per site across all individuals. We restricted the secondary lineage-specific filtering step to the subset of positions that were retained in the first round of filtering using the -sites option in ANGSD. Filtering in this manner guarantees that sites with an allele that is fixed in one lineage will be retained. The final population-specific filtered dataset was used to generate stairway plots, sliding window $F_{st}$ values, XP-CLR values, and to calculate $f_3$ statistics. *All-Sites Filtered Dataset.* The third dataset was filtered with the same method as the population-specific dataset, but we kept all positions including non-polymorphic sites. This dataset was used to calculate nucleotide diversity and $D_{XY}$ values.

**Population Structure Analysis**

We used the ngsDist option in ngsTools (70) on the LD-Filtered dataset to compute genetic distances between individuals and perform multiple dimensional scaling (MDS). We then looked for signatures of admixture using ngsAdmix (31) with runs ranging from K =2 to K = 7. Weighted pairwise $F_{ST}$s were estimated between the individuals from the North (Woods Hole, MA to Roanoke Island, NC) and the individuals from the South (Pivers Island, NC to Panacea, FL) using ANGSD with the `-doSaf 1` flag. We then used realSFS to estimate the 2D site frequency spectrum for each population and calculated the average pairwise weighted $F_{ST}$ using 'realSFS fst.' Weighted pairwise $F_{ST}$ estimates were also calculated between each sampling location using ANGSD with the same parameters.

NgsDist was used to compute genetic distances from genotype probabilities with *Bolinopsis infundibulum* as the outgroup (SRX14647678). Raw *Bolinopsis* sequences were filtered according to the same protocol as was applied to *Mnemiopsis* and then we ran ANGSD with *Bolinopsis* included, a minor allele frequency filter of 0.05 and a SNP pval filter of 1e-6. This set of filters resulted in 1,302 SNPs that were used to generate the phylogenetic tree based on the nuclear genome. NgsDist was run with 100 bootstrap replicates and a boot block size of 20. Finally, FastME v2.1.6.1 (71) was used to visualize the pairwise genetic distances and RAxML-NG v0.9.0 (72) was used to place bootstrap supports onto the tree. Final figures were generated using the interactive tree of life tool v6.9.1 (73).

Novoplasty v4.3.1 (74) was used to extract the mitochondrial genome from each trimmed sample using the published *Mnemiopsis leidyi* COI sequence (KF435121.1(75)). When this was unsuccessful, we instead used the published *Bolinopsis microptera* (SRX10473759 (46)) whole-genome sequences and ran Novoplasty with the published *B. microptera* COI seed (MW735734.1 (76)) to extract the complete mitochondrial genome. The complete *B. microptera* mitochondrial genome was then used as a seed for the remaining samples that initially failed Novoplasty. Using this approach, we were able to successfully assemble 112 out of 118 *Mnemiopsis* mitochondrial genomes. Next, we used MARS (77) to ensure that each mitochondrial genome began at the same location using the branch and bound method and the block length set to 100. We used MAFFT v7.480 (78) to generate an alignment and IQ-TREE v2.3.2 (79) to generate a phylogenetic tree.

**Demographic Analysis**

StairwayPlot v2 (33) was used to reconstruct effective population sizes based on the folded SFSs generated from the All-Sites Filtered dataset. We used a mutation rate of 6.85 x $10^{-8}$ per base pair per year (22) and a generation time of 1 year (80). A one-year generation time was chosen based on Charlesworth et al 1994 (81) who asserted that generation time can be estimated as the mean age at reproduction for a female. The hermaphroditic *Mnemiopsis* can reproduce within the first month of its lifespan (82) its lifespan is approximately 2 years (80) and there is no information indicating that they ever lose the ability to reproduce. As such a mean age of reproduction was set to 1 year.

**$F_3$ Statistics**

We used $f_3$ statistics, included as part of the ADMIXTOOLS package v.7.0.2 (32), as a direct test for detecting hybridization. The $f_3$ statistic estimates whether allele frequency differences between each population combination deviates more than expected because of incomplete lineage sorting, which implicates admixture. If the $f_3$ statistic is negative, this suggests that admixture has likely occurred. For this analysis, all populations which belonged to the northern mitochondrial lineage were combined into one population and all the populations which belonged to the southern mitochondrial lineage were combined into the second population. These two lineages were tested against Roanoke Island, NC and Gloucester Point, VA.

490
491 **Genomic Signatures of Selection**
492 To detect regions of the genome under natural selection between the two lineages, we used XP-
493 CLR (50) which uses the AFS to calculate local deviations between populations. We used a sliding
494 window and step size of 10kb with the maxSNPs flag set to 200. The genomic regions in the top
495 10% of the XP-CLR values were considered to represent selective sweeps and were associated
496 with overlapping genes using Bedtools v.2.29.0 (83). We conducted a Monte Carlo analysis to
497 identify overrepresented gene ontology terms as was conducted in Babonis et al. 2018 (84).
498
499 To further investigate genomic patterns of regions under selection, we generated sliding window
500 scans for $F_{ST}$, $D_{XY}$, and nucleotide diversity values. To generate the sliding window scans, we used
501 the population-specific filtered dataset with the Roanoke Island, NC population removed. We then
502 used realSFS $F_{ST}$ index in ANGSD to compute per-site $F_{ST}$ indexes and realSFS $F_{ST}$ stats2 to
503 perform a window-sliding analysis with the window and step size set to 10 kb to ensure
504 nonoverlapping windows. The All-Sites Filtered dataset, with the Roanoke Island population
505 removed, was used to generate nucleotide diversity and $D_{XY}$ values. For nucleotide diversity
506 calculations, we used realSFS saf2theta in ANGSD to generate folded SFS's and then generated
507 these values along a sliding window with thetaStat do_stat and the window and step size set to 10
508 kb. For $D_{XY}$ calculations, we used the CalcDxy.R code by Joshua Penalba then averaged the
509 resulting values over the same 10kb windows as the $F_{ST}$ and nucleotide calculations.
510
511 **Acknowledgements**
512 This work was funded with a Postdoctoral Research Fellowship in Biology (PRFB) from the
513 National Science Foundation (award number: 2109712). We would like to thank Dr. Ann Tarrant,
514 Roland Hagan, Robert Aguilar, Dr. Deborah Steinberg, Tor Mowatt-Larssen, Eli at Outer Banks
515 Kayaking Adventures, Dr. Joshua Osterberg, Dr. Jacob Warner, Dr. Daniel Sasson, Dr. Marc
516 Frischer, Dr. Adam Greer, Dr. Holly Sweat, and Dr. Yuriy Bobkov for help collecting *Mnemiopsis*
517 samples along the US Atlantic coast. We would like to acknowledge the ICBR for their excellent
518 sequencing and service (RRID:SCR_019152). We would like to thank Dr. James Thomas at the
519 NIH Intramural Sequencing Center (NISC) for his help with the PacBio sequencing. We would
520 also like to thank Dr. Gustav Paulay and Dr. Claudia Mills for their help navigating the complex
521 taxonomy of *Mnemiopsis*. Finally, we want to thank Dr. Mark Ravinet for his help brainstorming
522 ideas pertaining to the hybridization of these two lineages.
523
524 **Citations**
525
526 1. L. Q. Choo, *et al.*, Genome-wide phylogeography reveals cryptic speciation in the
527 circumglobal planktonic calcifier Limacina bulimoides. *Molecular Ecology* **32**, 3200–3219
528 (2023).

2. C. Breusing, *et al.*, Allopatric and Sympatric Drivers of Speciation in Alviniconcha Hydrothermal Vent Snails. *Mol Biol Evol* **37**, 3469–3484 (2020).

3. D. Schluter, D. J. Howard, S. H. Berlocher, *Endless forms: species and speciation* (Oxford Univ. Press, 1998).

4. M. P. Miglietta, A. Faucci, F. Santini, Speciation in the Sea: Overview of the Symposium and Discussion of Future Directions. *Integrative and Comparative Biology* **51**, 449–455 (2011).

5. C. Jaspers, J. H. Costello, S. P. Colin, Carbon content of Mnemiopsis leidyi eggs and specific egg production rates in northern Europe. *Journal of Plankton Research* **37**, 11–15 (2015).

6. T. Shiganova, Changes in appendicularian Oikopleura dioica abundance caused by invasion of alien ctenophores in the Black Sea. *Journal of the Marine Biological Association of the United Kingdom* **85**, 477–494 (2005).

7. H. W. Mianzan, P. Martos, J. H. Costello, R. A. Guerrero, Avoidance of hydrodynamically mixed environments by Mnemiopsis leidyi (Ctenophora: Lobata) in open-sea populations from Patagonia, Argentina. *Jellyfish Blooms: New Problems and Solutions* 113–124 (2010).

8. G. R. Harbison, S. P. Volovik, THE CTENOPHORE, MNEMIOPSIS LEIDYI, IN THE BLACK SEA: A HOLOPLANKTONIC ORGANISM TRANSPORTED in *Nonindigenous Estuarine & Marine Organisms (NEMO): Proceedings of the Conference and Workshop, Seattle, Washington, April 1993*, (US Department of Commerce, National Oceanic and Atmospheric Administration, 1994), p. 25.

9. H. W. Mianzan, P. Martos, J. H. Costello, R. A. Guerrero, Avoidance of hydrodynamically mixed environments by Mnemiopsis leidyi (Ctenophora: Lobata) in open-sea populations from Patagonia, Argentina. *Jellyfish Blooms: New Problems and Solutions* 113–124 (2010).

10. S. Lowe, M. Browne, S. Boudjelas, M. De Poorter, *100 of the world's worst invasive alien species: a selection from the global invasive species database* (Invasive Species Specialist Group Auckland, 2000).

11. L. Doyle, Mnemiopsis leidyi. *AN INTRODUCTION TO MARINE INVASIVE SPECIES* **52** (1984).

12. T. A. Shiganova, Adaptive strategies of Mnemiopsis leidyi A. Agassiz 1865 in different environments of the Eurasian seas. *Marine Pollution Bulletin* **161**, 111737 (2020).

13. C. Jaspers, L. F. Møller, T. Kiørboe, Reproduction rates under variable food conditions and starvation in Mnemiopsis leidyi: significance for the invasion success of a ctenophore. *Journal of Plankton Research* **37**, 1011–1018 (2015).

14. A. Edgar, D. G. Mitchell, M. Q. Martindale, Whole-body regeneration in the lobate ctenophore Mnemiopsis leidyi. *Genes* **12**, 867 (2021).

15. D. A. Sasson, J. F. Ryan, The sex lives of ctenophores: the influence of light, body size, and self-fertilization on the reproductive output of the sea walnut, Mnemiopsis leidyi. *PeerJ* **4**, e1846 (2016).

16. D. A. Sasson, A. A. Jacquez, J. F. Ryan, The ctenophore Mnemiopsis leidyi regulates egg production via conspecific communication. *BMC Ecology* **18**, 1–10 (2018).

17. C. M. Child, The gradient in susceptibility to cyanides in the meridional conducting path of the ctenophore Mnemiopsis. *American Journal of Physiology-Legacy Content* **43**, 87–112 (1917).

18. J. F. Ryan, *et al.*, The genome of the ctenophore Mnemiopsis leidyi and its implications for cell type evolution. *Science* **342**, 1242592 (2013).

19. R. T. Moreland, *et al.*, A customized Web portal for the genome of the ctenophore Mnemiopsis leidyi. *BMC Genomics* **15**, 1–13 (2014).

20. R. T. Moreland, A.-D. Nguyen, J. F. Ryan, A. D. Baxevanis, The Mnemiopsis Genome Project Portal: integrating new gene expression resources and improving data visualization. *Database* **2020**, baaa029 (2020).

21. R. T. Moreland, S. Zhang, S. N. Barreira, J. F. Ryan, A. D. Baxevanis, An AI-generated proteome-scale dataset of predicted protein structures for the ctenophore Mnemiopsis leidyi. *Proteomics* 2300397 (2024).

22. C. Jaspers, *et al.*, Invasion genomics uncover contrasting scenarios of genetic diversity in a widespread marine invader. *Proceedings of the National Academy of Sciences* **118**, e2116211118 (2021).

23. K. M. Bayha, *et al.*, Worldwide phylogeography of the invasive ctenophore Mnemiopsis leidyi (Ctenophora) based on nuclear and mitochondrial DNA data. *Biological Invasions* **17**, 827–850 (2015).

24. C. Verwimp, *et al.*, Population genomic structure of the gelatinous zooplankton species Mnemiopsis leidyi in its nonindigenous range in the North Sea. *Ecology and Evolution* **10**, 11–25 (2020).

25. T. B. Reusch, S. Bolte, M. Sparwel, A. G. Moss, J. Javidpour, Microsatellites reveal origin and genetic diversity of Eurasian invasions by one of the world's most notorious marine invader, Mnemiopsis leidyi (Ctenophora). *Molecular ecology* **19**, 2690–2699 (2010).

26. J. M. Pujolar, D. Breitburg, J. Lee, M. B. Decker, C. Jaspers, Hybridization and adaptive introgression in a marine invasive species in native habitats. *Iscience* **26** (2023).

27. S. Ahyong, *et al.*, World Register of Marine Species (WoRMS). WoRMS Editorial Board. Deposited 14 September 2024.

28. L. N. Seravin, The systematic revision of the genus Mnemiopsis (Ctenophora, Lobata). *Zoologičeskij žurnal* **73**, 9–18 (1994).

29. M. Domènech, L. C. Crespo, A. Enguídanos, M. A. Arnedo, Mitochondrial discordance in closely related Theridion spiders (Araneae, Theridiidae), with description of a new species of the T. melanurum group. *Zoosystematics and Evolution* **96**, 159–173 (2020).

30. D. W. Foltz, *et al.*, Global population divergence of the sea star Hippasteria phrygiana corresponds to the onset of the last glacial period of the Pleistocene. *Marine Biology* **160**, 1285–1296 (2013).

31. L. Skotte, T. S. Korneliussen, A. Albrechtsen, Estimating individual admixture proportions from next generation sequencing data. *Genetics* **195**, 693–702 (2013).

32. N. Patterson, *et al.*, Ancient Admixture in Human History. *Genetics* **192**, 1065–1093 (2012).

33. X. Liu, Y.-X. Fu, Stairway Plot 2: demographic history inference with folded SNP frequency spectra. *Genome Biology* **21**, 280 (2020).

34. H. (Kikki) F. Kleiven, *et al.*, Reduced North Atlantic deep water coeval with the glacial Lake Agassiz freshwater outburst. *science* **319**, 60–64 (2008).

35. J. T. Teller, D. W. Leverington, J. D. Mann, Freshwater outbursts to the oceans from glacial Lake Agassiz and their role in climate change during the last deglaciation. *Quaternary Science Reviews* **21**, 879–887 (2002).

36. L. Martínez-García, *et al.*, Historical demographic processes dominate genetic variation in ancient Atlantic cod mitogenomes. *Frontiers in Ecology and Evolution* **9**, 671281 (2021).

37. L. M. Atmore, *et al.*, Population dynamics of Baltic herring since the Viking Age revealed by ancient DNA and genomics. *Proceedings of the National Academy of Sciences* **119**, e2208703119 (2022).

38. H. Li, R. Durbin, Inference of human population history from individual whole-genome sequences. *Nature* **475**, 493–496 (2011).

39. X. Liu, Y.-X. Fu, Exploring population size changes using SNP frequency spectra. *Nature genetics* **47**, 555–559 (2015).

40. M. Manni, M. R. Berkeley, M. Seppey, E. M. Zdobnov, BUSCO: assessing genomic data quality and beyond. *Current Protocols* **1**, e323 (2021).

41. N. H. Putnam, *et al.*, Sea anemone genome reveals ancestral eumetazoan gene repertoire and genomic organization. *science* **317**, 86–94 (2007).

42. N. H. Putnam, *et al.*, The amphioxus genome and the evolution of the chordate karyotype. *Nature* **453**, 1064–1071 (2008).

43. O. Simakov, *et al.*, Insights into bilaterian evolution from three spiralian genomes. *Nature* **493**, 526–531 (2013).

44. D. T. Schultz, *et al.*, Ancient gene linkages support ctenophores as sister to other animals. *Nature* **618**, 110–117 (2023).

45. T. D. Lewin, I. J.-Y. Liao, Y.-J. Luo, Annelid comparative genomics and the evolution of massive lineage-specific genome rearrangement in bilaterians. *Molecular Biology and Evolution* **41**, msae172 (2024).

46. S. B. Johnson, *et al.*, Speciation of pelagic zooplankton: Invisible boundaries can drive isolation of oceanic ctenophores. *Frontiers in Genetics* **13**, 970314 (2022).

47. L. D. Talley, M. S. McCartney, Distribution and circulation of Labrador Sea water. *Journal of Physical Oceanography* **12**, 1189–1205 (1982).

48. B. Gaylord, S. D. Gaines, Temperature or transport? Range limits in marine species mediated solely by flow. *The American Naturalist* **155**, 769–789 (2000).

49. K. Matsumoto, J. Lynch-Stieglitz, Persistence of Gulf Stream separation during the Last Glacial Period: Implications for current separation theories. *Journal of Geophysical Research: Oceans* **108** (2003).

50. H. Chen, N. Patterson, D. Reich, Population differentiation as a test for selective sweeps. *Genome research* **20**, 393–402 (2010).

51. M. Ashburner, *et al.*, Gene ontology: tool for the unification of biology. *Nature Genetics* **25**, 25–29 (2000).

653 52. C.-R. Torres, G. W. Hart, Topography and polypeptide distribution of terminal N-
654 acetylglucosamine residues on the surfaces of intact lymphocytes. Evidence for O-linked
655 GlcNAc. *Journal of Biological Chemistry* **259**, 3308–3317 (1984).

656 53. B. Guo, *et al.*, O-GlcNAc-modification of SNAP-29 regulates autophagosome maturation.
657 *Nature Cell Biology* **16**, 1215–1226 (2014).

658 54. N. Mizushima, Sugar modification inhibits autophagosome–lysosome fusion. *Nature Cell*
659 *Biology* **16**, 1132–1133 (2014).

660 55. M. Ehrlich, "Invasion Genomics: population structure and diversity patterns in the invasive
661 ctenophore Mnemiopsis leidyi based on whole-genome re-sequencing," Christian-
662 Albrechts-Universität Kiel. (2017).

663 56. H. Cheng, G. T. Concepcion, X. Feng, H. Zhang, H. Li, Haplotype-resolved de novo
664 assembly using phased assembly graphs with hifiasm. *Nature methods* **18**, 170–175 (2021).

665 57. M. J. Roach, S. A. Schmidt, A. R. Borneman, Purge Haplotigs: allelic contig reassignment
666 for third-gen diploid genome assemblies. *BMC Bioinformatics* **19**, 1–10 (2018).

667 58. J. M. Flynn, *et al.*, RepeatModeler2 for automated genomic discovery of transposable
668 element families. *Proceedings of the National Academy of Sciences* **117**, 9451–9457
669 (2020).

670 59. B. Langmead, S. L. Salzberg, Fast gapped-read alignment with Bowtie 2. *Nature methods*
671 **9**, 357–359 (2012).

672 60. T. Brůna, K. J. Hoff, A. Lomsadze, M. Stanke, M. Borodovsky, BRAKER2: automatic
673 eukaryotic genome annotation with GeneMark-EP+ and AUGUSTUS supported by a
674 protein database. *NAR genomics and bioinformatics* **3**, lqaa108 (2021).

675 61. B. Buchfink, K. Reuter, H.-G. Drost, Sensitive protein alignments at tree-of-life scale using
676 DIAMOND. *Nature methods* **18**, 366–368 (2021).

677 62. S. El Hilali, R. R. Copley, macrosyntR: Drawing automatically ordered Oxford Grids from
678 standard genomic files in R. *bioRxiv* 2023.01. 26.525673 (2023).

679 63. A. M. Bolger, M. Lohse, B. Usadel, Trimmomatic: a flexible trimmer for Illumina sequence
680 data. *Bioinformatics* **30**, 2114–2120 (2014).

681 64. H. Li, *et al.*, The sequence alignment/map format and SAMtools. *bioinformatics* **25**, 2078–
682 2079 (2009).

683 65. A. Tarasov, A. J. Vilella, E. Cuppen, I. J. Nijman, P. Prins, Sambamba: fast processing of
684 NGS alignment formats. *Bioinformatics* **31**, 2032–2034 (2015).

685 66. G. Jun, M. K. Wing, G. R. Abecasis, H. M. Kang, An efficient and scalable analysis
686 framework for variant extraction and refinement from population-scale DNA sequence
687 data. *Genome research* **25**, 918–925 (2015).

688 67. T. S. Korneliussen, A. Albrechtsen, R. Nielsen, ANGSD: analysis of next generation
689 sequencing data. *BMC bioinformatics* **15**, 1–13 (2014).

690 68. E. A. Fox, A. E. Wright, M. Fumagalli, F. G. Vieira, ngsLD: evaluating linkage
691 disequilibrium using genotype likelihoods. *Bioinformatics* **35**, 3855–3856 (2019).

692 69. R. N. Lou, A. Jacobs, A. P. Wilder, N. O. Therkildsen, A beginner's guide to low-coverage
693 whole genome sequencing for population genomics. *Molecular Ecology* **30**, 5966–5993
694 (2021).

695 70. M. Fumagalli, F. G. Vieira, T. Linderoth, R. Nielsen, ngsTools: methods for population
696 genetics analyses from next-generation sequencing data. *Bioinformatics* **30**, 1486–1487
697 (2014).

698 71. V. Lefort, R. Desper, O. Gascuel, FastME 2.0: a comprehensive, accurate, and fast
699 distance-based phylogeny inference program. *Molecular biology and evolution* **32**, 2798–
700 2800 (2015).

701 72. A. M. Kozlov, D. Darriba, T. Flouri, B. Morel, A. Stamatakis, RAxML-NG: a fast, scalable
702 and user-friendly tool for maximum likelihood phylogenetic inference. *Bioinformatics* **35**,
703 4453–4455 (2019).

704 73. I. Letunic, P. Bork, Interactive Tree of Life (iTOL) v6: recent updates to the phylogenetic
705 tree display and annotation tool. *Nucleic Acids Research* gkae268 (2024).

706 74. N. Dierckxsens, P. Mardulyn, G. Smits, NOVOPlasty: de novo assembly of organelle
707 genomes from whole genome data. *Nucleic acids research* **45**, e18–e18 (2017).

708 75. S. Ghabooli, *et al.*, Invasion pathway of the ctenophore Mnemiopsis leidyi in the
709 Mediterranean Sea. *PloS one* **8**, e81067 (2013).

710 76. L. M. Christianson, S. B. Johnson, D. T. Schultz, S. H. Haddock, Hidden diversity of
711 Ctenophora revealed by new mitochondrial COI primers and sequences. *Molecular Ecology*
712 *Resources* **22**, 283–294 (2022).

713 77. L. A. Ayad, S. P. Pissis, MARS: improving multiple circular sequence alignment using
714 refined sequences. *BMC genomics* **18**, 1–10 (2017).

715 78. K. Katoh, D. M. Standley, MAFFT multiple sequence alignment software version 7:
716 improvements in performance and usability. *Molecular biology and evolution* **30**, 772–780
717 (2013).

718 79. B. Q. Minh, *et al.*, IQ-TREE 2: new models and efficient methods for phylogenetic
719 inference in the genomic era. *Molecular biology and evolution* **37**, 1530–1534 (2020).

720 80. J. S. Presnell, M. Bubel, T. Knowles, W. Patry, W. E. Browne, Multigenerational laboratory
721 culture of pelagic ctenophores and CRISPR–Cas9 genome editing in the lobate Mnemiopsis
722 leidyi. *Nature Protocols* **17**, 1868–1900 (2022).

723 81. B. Charlesworth, *Evolution in age-structured populations* (Cambridge University Press
724 Cambridge, 1994).

725 82. A. Edgar, J. M. Ponciano, M. Q. Martindale, Ctenophores are direct developers that
726 reproduce continuously beginning very early after hatching. *Proceedings of the National*
727 *Academy of Sciences* **119**, e2122052119 (2022).

728 83. A. R. Quinlan, I. M. Hall, BEDTools: a flexible suite of utilities for comparing genomic
729 features. *Bioinformatics* **26**, 841–842 (2010).

730 84. L. S. Babonis, *et al.*, Integrating embryonic development and evolutionary history to
731 characterize tentacle-specific cell types in a ctenophore. *Molecular Biology and Evolution*
732 **35**, 2940–2956 (2018).